RSC Advances

PAPER

View Article Online
View Journal | View Issue

Cite this: *RSC Adv.*, 2018, **8**, 18197

Functionalization of composite bacterial cellulose with C_{60} nanoparticles for wound dressing and cancer therapy†

Minglei Chu,‡[ab] Huichang Gao,‡[d] Sa Liu,*[ac] Lin Wang,[ac] Yongguang Jia,[ac] Meng Gao,[ac] Miaojian Wan,[e] Chengfang Xu[e] and Li Ren*[ac]

A series of novel bacterial cellulose/C_{60} (BCC_{60}) composites was prepared using a original dehydration-rehydration method. The composites were characterized to demonstrate their potential in multifunctional wound dressings for skin cancer treatment using photodynamic therapy. Raman spectroscopy revealed that the C_{60} nanoparticles were successfully incorporated into the bacterial cellulose (BC) network. Scanning electron microscopy was used to examine the morphology and distribution of the C_{60} particles as photosensitizers in the bacterial cellulose network, and the C_{60} particles were uniformly distributed in the hyperfine three-dimensional BC network with diameters less than 100 nm. Reactive oxygen species (ROS) measurements indicated that the BCC_{60} composites possessed a high ROS generation ability when exposed to light. The antibacterial assessment of the BCC_{60} composites revealed their ability to inhibit the growth of *E. coli* and *S. aureus* and their relationship with light irradiation. *In vitro* cell experiments also confirmed that the BCC_{60} composites had low cytotoxicity in the dark, while they exhibited significant cancer cell damage activity under visible light.

Received 7th January 2018
Accepted 9th May 2018

DOI: 10.1039/c8ra03965h

rsc.li/rsc-advances

Introduction

In recent years, cancer has become increasingly common as a result of environmental pollution. However, traditional cancer therapies involving surgery, chemotherapy and radiation therapy lead to serious side effects, including great trauma and damage to the immune system and normal tissues.[1] Photodynamic therapy (PDT), as a milder and safer treatment, has attracted much attention by researchers and can generate reactive oxygen species (ROS) to cause cancer cell damage *via* the combination of visible light, oxygen and a photosensitizer.[2]

Currently, photosensitizers, as one of the determinants of the effectiveness of PDT for cancer, mainly consist of porphyrinoid photosensitizers, non-porphyrinoid photosensitizers, 5-aminolevulinic acid, fullerenes and their derivatives.[3] Reports have indicated that the former three types do not exhibit good water solubility, photostability, acceptable skin photosensitization or the desired biodistribution. Fullerenes and their derivatives, such as C_{60}, are attracting increased attention and application in PDT.

C_{60}, an effective photosensitizer for PDT, yields a highly reactive singlet oxygen ($^1O_2$), with generation rates reaching 95%.[4] In addition, C_{60} exhibits non-cytotoxicity without light irradiation, drawing the attention of several researchers.[5] However, the poor solubility of C_{60} in polar solvents has hampered its application in PDT.[6] Although the chemical modification of C_{60} with hydrophilic groups can improve its solubility, the process leads to aggregation and decreases the ROS generation rate by an order of magnitude.[7] For example, T. Andersson and K. Komatsu had fabricated C_{60}-(γ-CD)$_2$ and C_{70}-(γ-CD)$_2$ by host–guest interaction,[8,9] and found that C_{70} exhibited high photodynamic activity while it didn't after treated with C_{60}-(γ-CD)$_2$. M. Akiyama had adopted the block copolymer micelles with different surface charge to load the C_{60} and found that only the C_{60} entrapped by positive charged block copolymer micelle exhibited cytotoxicity towards HeLa cells after irradiation.[10] At present, for the application of C_{60}, there is an urgent need for more efficient methods to be developed. In this study, we developed a novel method to improve the efficiency of C_{60} as a photosensitizer by combining the BC and C_{60} to form the BCC_{60} composites. BC, a hydrogel secreted by bacteria, was considered as an alternative carrier of C_{60}, which result from that BC possesses good biocompatibility and excellent mechanical and optical properties[11] and, hence, can

[a]*School of Materials Science and Engineering, South China University of Technology, Guangzhou 510641, China. E-mail: psliren@scut.edu.cn*
[b]*Center for Medical Device Evaluation, China Food and Drug Administration, Beijing 100081, China*
[c]*A National Engineering Research Centre for Tissue Restoration and Reconstruction, Guangzhou 510006, China*
[d]*School of Medicine, South China University of Technology, Guangzhou 510006, China*
[e]*The Third Affiliated Hospital, Sun Yat-Sen University, Guangzhou 510630, China*

† Electronic supplementary information (ESI) available. See DOI: 10.1039/c8ra03965h

‡ These authors contributed equally to this work.

meet the requirements of C_{60} carriers to fabricate a multifunctional wound dressing as a new form of PDT.

In this study, to improve the efficiency of C_{60} as a photosensitizer, bacterial cellulose (BC), a hydrogel secreted by bacteria, was considered as an alternative carrier of C_{60} in the form of a multifunctional wound dressing. It has been reported that BC possesses good biocompatibility and other physical and chemical properties, especially the excellent mechanical property, swelling ability optical properties[11] and gas transmission, hence, can meet the requirements of C_{60} carriers for a new form of PDT.

In the present study, a solvent exchange method was used to prepare a C_{60} water suspension, which has been reported to have a high ROS regeneration ability, with tetrahydrofuran (THF) as the organic solvent.[12] Here, a dehydration-rehydration method was invented to load C_{60} onto BC successfully. The antibacterial abilities and cytotoxicity toward human-derived epidermoid carcinoma cells (A-431 cell line) of the resulting composites are evaluated. This paper aims to develop the composites for use in multifunctional wound dressings to treat skin cancer by PDT (Fig. 1).

Materials and methods

Preparation and purification of the BC

As described in previous studies,[11] the BC membrane was prepared through the static cultivation of *Acetobacter xylinus* (ATCC, USA) on a sterilized liquid medium containing fermented coconut juice, 1% yeast extract powder, 0.6% peptone, 0.02% $MgSO_4$, 0.01% $CaCl_2$ and 2% glucose. Subsequently, the BC membrane was purified by sequential washing steps with tap water, distilled water, 0.1 M NaOH, 2% sodium dodecyl sulfate and distilled water. The purified BC membranes were sheared into 15 mm discs and stored in deionized water at low temperature to prevent drying.

Preparation of the C_{60} water suspension

The C_{60} water suspension, nC_{60}, was prepared using the modified THF method described previously.[12–14] Briefly, 10 mg of 99.9% pure C_{60} nanoparticles (Aladdin, Shanghai, China) was dissolved in 1 L of unopened anhydrous THF (99.9%+, inhibitor-free, Aladdin, Shanghai, China) followed by stirring for 72 h in the dark at room temperature. The undissolved C_{60} particles were removed after filtration through a 0.45 μm nylon membrane (Anpel, Shanghai, China) to obtain the C_{60} saturated THF solution. An equal amount of Milli-Q water (Millipore, USA) was added at a rate of 1 L min^{-1}. Then, the evaporation step was conducted using a rotary evaporator (RE-2000B, Shanghai Yarong Biochemical Instrument Factory, Shanghai, China) to completely remove the THF at 55 °C and most of the water at 80 °C to obtain a final volume of approximately 50 mL. The obtained brownish-yellow water suspension, nC_{60}, was diluted to the proper concentration. After sterilization using ultraviolet light irradiation, the C_{60} water suspension was stored at 4 °C before use.

Preparation of the BCC_{60} composites

The BCC_{60} composites were prepared using a dehydration-rehydration method with a vacuum filtration system containing a Buchner funnel, a filtering flask and a vacuum pump. Naturally dehydrated BC with a diameter larger than Buchner

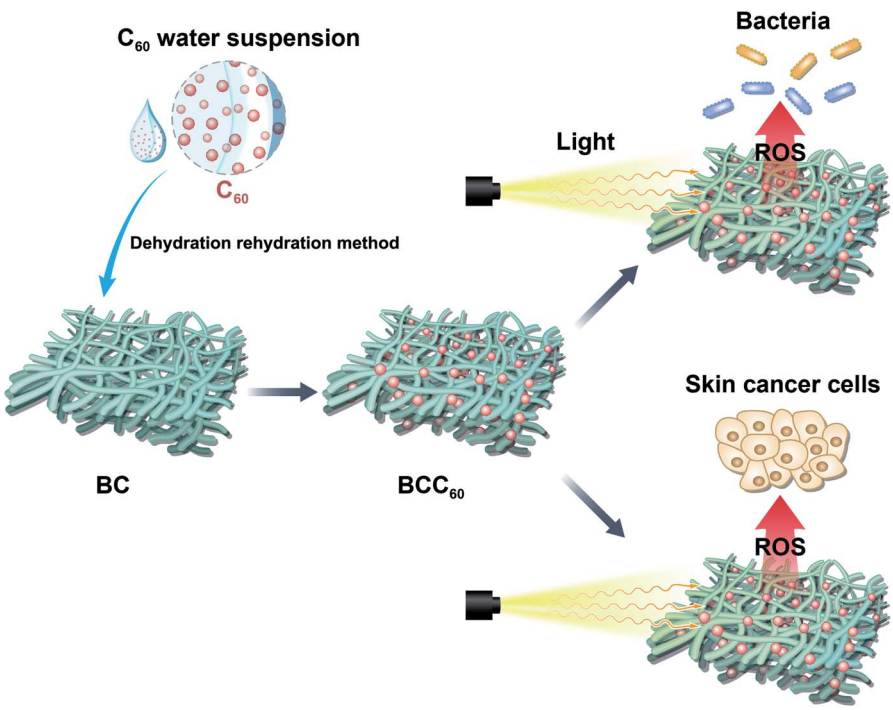

Fig. 1 Illustration of the BCC_{60} composite preparation and application.

funnel was spread over the Buchner funnel. The diluted nC$_{60}$ with different concentrations were pulled onto the BC followed by vacuuming to help adsorb the C$_{60}$ onto the BC. The above steps were repeated three times to complete the composite formation. Finally, the obtained BCC$_{60}$ composites were sterilized by ultraviolet light irradiation and stored at 4 °C before use.

Raman spectra

The chemical structures of the BCC$_{60}$ composites were characterized using Raman spectra (CCD-7949, Horiba Jobin Yvon, France) in the range between 400 cm^{-1} and 4000 cm^{-1} to observe the combination of BC and C$_{60}$ after lyophilization and being ground into a powder.

Morphology of the BCC$_{60}$ composites

Scanning electron microscopy (SEM, EVO18, Germany) was used to characterize the morphology of the prepared BCC$_{60}$ materials. Prior to the SEM observations, the prepared composites were lyophilized and coated with an ultrathin layer of gold by ion sputtering.

ROS measurements

An electron paramagnetic resonance (EPR) spectrometer was used to detect the ROS generation from composite extracts *in vitro* using 2,2,6,6-tetramethylpiperidine (TEMP, Sigma, 115754, USA) as the capture agent.[12] In brief, the BCC$_{60}$ composites were immersed in PBS at 37 °C for 12 h to prepare the BCC$_{60}$ extracts. The ROS capture agent TEMP was added to the BCC$_{60}$ extracts followed by light irradiation, whereas pure TEMP was utilized as the control group.

To identify the different ROS generated from the composites with different contents of C$_{60}$, another indirect detection method was used, as previously reported.[15,16] In brief, materials with a certain diameter were treated with DCFH-DA (Sigma, D6883, 38297 Saint Quentin Fallavier, France) with a final concentration of 40 μM followed by persistent white light irradiation. The fluorescence intensity was assessed using a microplate reader (Thermo 3001, USA) at 485 nm for excitation and 530 nm for emission for intervals of five minutes.

Antibacterial assessment

The colony forming count method[17–19] was used to assess the antibacterial properties of the BC and BCC$_{60}$ composites against *Escherichia coli* and *Staphylococcus aureus*. *E. coli* and *S. aureus* were purchased from the Guangzhou Industrial Microbiology Testing Center (Guangzhou, China). After cultivation in a nutrient broth, the bacteria were seeded onto the material in 24-well culture plates with 300 μL of the bacterial suspension (1.0×10^6 cfu mL^{-1}). The experiments were split between light groups and dark groups. After inoculation for 2 h at 37 °C, whether exposed to white light or not, the bacteria were diluted and coated on agar plates to count the colonies visually after culturing for 12 h at 37 °C. We used the following equation to measure the antibacterial rate:

$$A = (C_t - C_0)/C_t \times 100\% \quad (1)$$

where C_t represents the colony number of the experiment group and C_0 represents the colony number of the control group.

Phototoxicity

Phototoxicity was measured with the widely used CCK-8 cell counting kit (CCK-8, Dojindo Laboratories, Japan). The experiments were divided into a light group and dark group. All the materials were separated into five groups: BC, BCC$_{60}$-005, BCC$_{60}$-010, BCC$_{60}$-050 and BCC$_{60}$-100. Each group had six parallel samples. In detail, human-derived epidermoid carcinoma cells (A-431, Cell Bank of the Chinese Academy of Sciences, Shanghai, China) were propagated in Dulbecco's modified Eagle's medium (DMEM, Life Technologies, Gibco, USA) with 10% fetal bovine serum (FBS, Life Technologies, Gibco, USA). The BC and BCC$_{60}$ composites were placed in 24-well plates after being sterilized in an autoclave (HIYAMAMA HVA-110, Japan). The A-431 cells were seeded on the composites at a density of 3.0×10^5 cells per well and inoculated for 1 d at 37 °C in an incubator with 5% CO_2. After that, white light was irradiated on the light group for 1 h, while the dark group remained in the dark. At the determined time points, the CCK-8 working solution (DMEM : CCK-8 = 10 : 1) was added to each sample and incubated at 37 °C for 1 h. Subsequently, the supernatant medium was extracted, and the absorbance of the CCK-8 working solution was measured at 450 nm using a microplate reader (Thermo 3001, USA).

In addition, living/dead staining was carried out to observe the A-431 cell morphology on the BCC$_{60}$ composites using a laser scanning confocal microscope (CLSM, Leica SP8, Germany). Briefly, after culturing for 1 d, the A-431 cells were washed with PBS and then stained for 20 min at room temperature by adding the living/dead staining solution. After washing again with PBS, the cell viability and morphology of the A-431 cells on the surface of the composites was observed using a laser scanning confocal microscope.

Statistical analysis

A one-way analysis of variance (ANOVA) followed by Tukey's test for means comparison was used to assess the level of significance, employing SPSS 19.0 statistical software. The results were expressed as the mean ± standard error.

Results and discussion

Raman spectra

In this study, the dehydration-rehydration method was used to fabricate BCC$_{60}$ composites with a vacuum filtration system. To confirm that C$_{60}$ successfully penetrated into the BC, a Raman analysis was executed to characterize the π-conjugation bonds of C$_{60}$ after attaching to the BC. Fig. 2 shows that a new absorption peak at 1455 cm^{-1} appeared for the BCC$_{60}$ composites, while it did not appear for the pristine BC, which demonstrated that C$_{60}$ successfully formed a composite with the BC network.

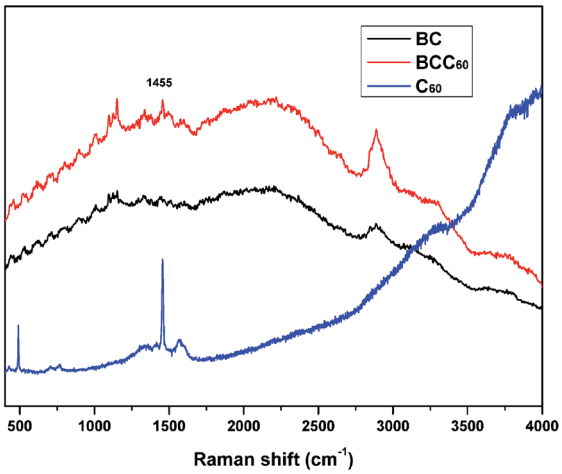

Fig. 2 Raman spectra of the BC, C_{60} and BCC_{60} composites.

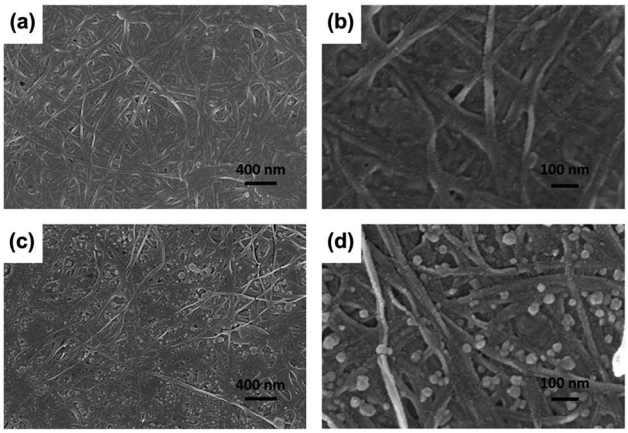

Fig. 3 SEM images of the BC and BCC_{60} composites (a) BC, X 30k; (b) BC, X 100k; (c) BCC_{60}, X 30k; (d) BCC_{60}, X 100k.

Morphology

SEM was used to further characterize the distribution and morphology of C_{60} in the BC network. As shown in Fig. 3, a three-dimensional fibrous network structure was observed in both the BC and BCC_{60}. Fig. 3c and d show that the C_{60} particles were uniformly distributed on the surface of the BC hyperfine three-dimensional network without apparent aggregation. In addition, the diameter of the C_{60} particles we prepared was much lower than 100 nm (Fig. 3d), reaching a smaller size than that in the previously reported literature.[20,21] The smaller size and reduced aggregation were more advantageous for enhancing ROS generation in the BCC_{60} composites for applications in PDT. These results showed that the hybrid process of BCC_{60} we adapted was suitable, and the BC may be an outstanding carrier of C_{60} as a multifunctional wound dressing.

ROS measurements

C_{60} is an effective photosensitizer in photodynamic therapy and yields highly reactive singlet oxygen ($^1O_2$). In the present study, due to its excellent transparency,[22,23] pristine BC was used to form a composite with C_{60} for PDT applications. After combining the BC with C_{60}, we characterized the ROS generation ability of the BCC_{60} composites under light irradiation. When irradiated with light, the BCC_{60} generated abundant ROS that could react with the capture agent TEMP to form TEMPO, which is known for its paramagnetism as an electron spin marker and can be detected using an electron paramagnetic resonance spectrometer; pure TEMP generates few ROS after irradiation.[24,25] The results are shown in Fig. 4. The BCC_{60} extracts effectively generated ROS, as shown in Fig. 4(a) and (b). DCF fluorescence was also measured to compare the production of ROS generated among the BCC_{60} composites with different contents of C_{60}. As shown in Fig. 4(c), the BCC_{60} composites with a higher C_{60} content generated ROS more effectively. In addition, with the increase in the light irradiation time, the intensity of the DCF fluorescence in the BCC_{60} composites had a strong positive correlation to the C_{60} content, while that of the control group increased only slightly. Taken together, these results showed that the BCC_{60} composites possessed the ability to generate ROS, and the yield of the ROS increased with the increased C_{60} content, which demonstrated that the great potential for application in PDT.

Antibacterial assessment

For wound healing, the antibacterial properties of biomaterials are a major standard for defining an eligible wound dressing.[26] PDT is a method for endowing enhanced antibacterial properties to materials with C_{60} photosensitizers. To assess this ability, the antibacterial efficacy of BC and BCC_{60} against *S. aureus* (Fig. 5) and *E. coli* (Fig. 6) was measured in light and dark conditions. As shown in Fig. 5 and 6, the BCC_{60} composites exhibited low antibacterial properties in the dark against both bacteria, which was enhanced with increasing C_{60} content. However, with light irradiation, the antibacterial properties were improved enormously, and the composites possessed excellent antibacterial abilities. In addition, as shown in Fig. 5b and 6b, the antibacterial ability of the BCC_{60} composites increased with the increasing C_{60} content under light irradiation, and the highest antibacterial rate reached 95%, while the highest antibacterial rate in the dark only reached 50%. This discrepancy may be related to different mechanisms of antibacterial efficacy in the different environments. It has been reported that, in a dark environment, C_{60} nanoparticles can pierce bacterial cell membranes, causing the cytoplasm to leak, resulting in slight antibacterial properties. However, light irradiation can induce C_{60} to react with oxygen from the atmosphere to generate abundant ROS, resulting in a boost in antibacterial efficacy.[27,28] Associated with the ROS measurements, materials with higher C_{60} content have better ROS generation ability, which means the higher antibacterial efficacy. In this work, as a transparent substrate, BC was chosen as the carrier of C_{60} for PDT applications to improve the antibacterial efficacy under light irradiation.

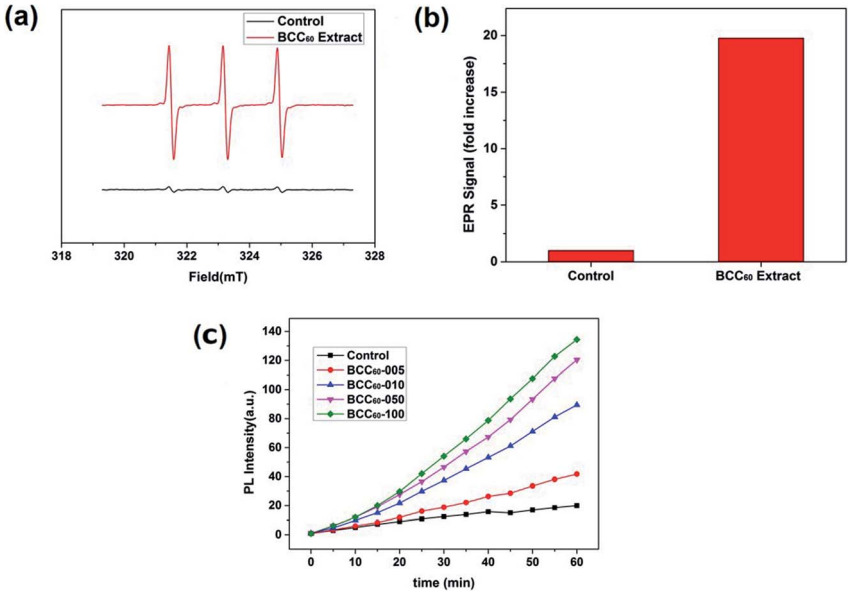

Fig. 4 ROS measurements of the BCC_{60} composites. (a) and (b) EPR spectra of the BCC_{60} extract. (c) DCF fluorescence of the BCC_{60} composites with varying C_{60} contents after irradiation.

Phototoxicity

Compared with the traditional cancer therapies, PDT is a novel and safer treatment that has attracted much attention from researchers and has the potential to exhibit high antibacterial rates and therapeutic effects for treating skin cancer. Therefore, the anti-cancer cell ability of the BCC_{60} composites was investigated in this work. Human-derived epidermoid carcinoma cells (A-431) were chosen as model skin cancer cells to characterize the anticancer effects of the BCC_{60} composite.

Similar to the antibacterial method, we also adapted two culture conditions, light and dark, to compare the different anticancer effects caused by the ROS generation. It has been reported that C_{60} is an effective photosensitizer that can release abundant ROS to kill cancer cells in the presence of light and oxygen. To determine the possible dosage effects of C_{60}, we selected different BCC_{60} composites prepared with varying concentrations of C_{60} suspensions. The A-431 cells were seeded on the BCC_{60} composites and cultured for 24 h, as described above. The results are shown in Fig. 7 and 8 and indicate that

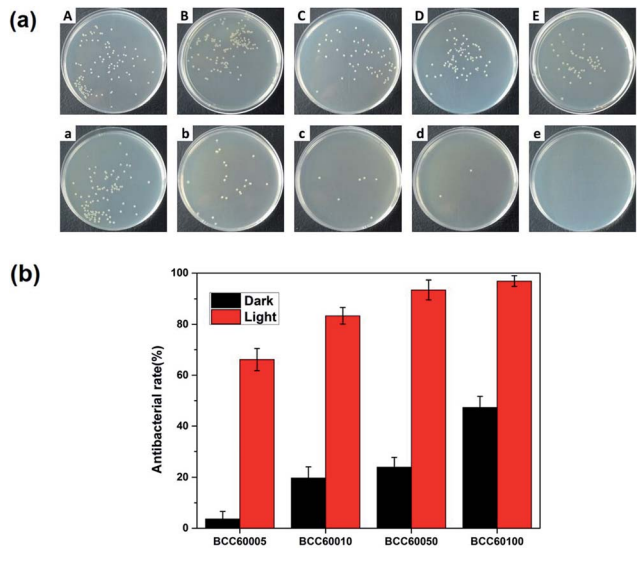

Fig. 5 (a) Antibacterial efficacy of the BC and BCC_{60} composites against *S. aureus* without (A–E) and with (a–e) light irradiation. (A and a) BC, (B and b) BCC_{60}-005, (C and c) BCC_{60}-010, (D and d) BCC_{60}-050, and (E and e) BCC_{60}-100. (b) Antibacterial rate of BCC_{60} against *S. aureus*.

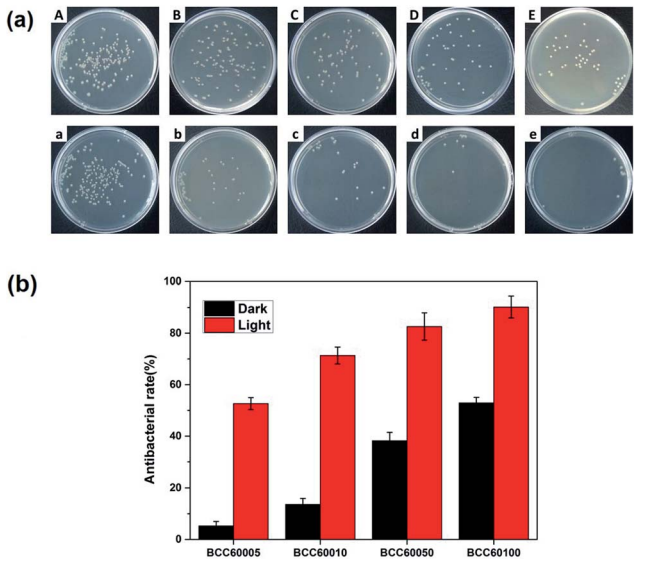

Fig. 6 (a) Antibacterial efficacy of the BC and BCC_{60} composites against *E. coli* without (A–E) and with (a–e) light irradiation. (A, a) BC, (B, b) BCC_{60}-005, (C, c) BCC_{60}-010, (D, d) BCC_{60}-050, and (E, e) BCC_{60}-100. (b) Antibacterial rate of BCC_{60} against *E. coli*.

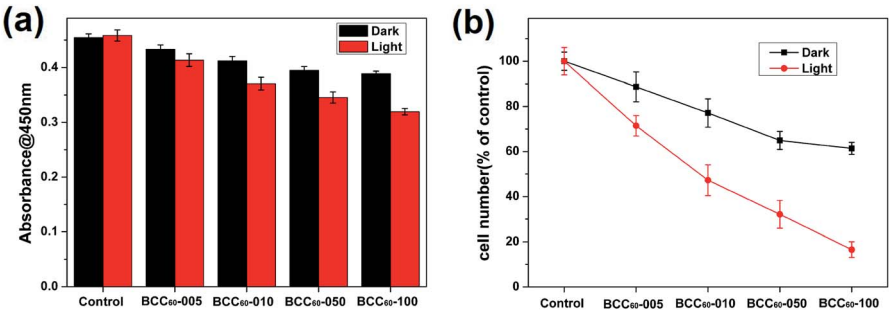

Fig. 7 Proliferation of A-431 cells seeded on the BC and BCC_{60} composites. Cell proliferation behavior (a) and cell number (b) measured with the CCK-8 assay after culturing A-431 cells on the BC and BCC_{60} composites for 1 d.

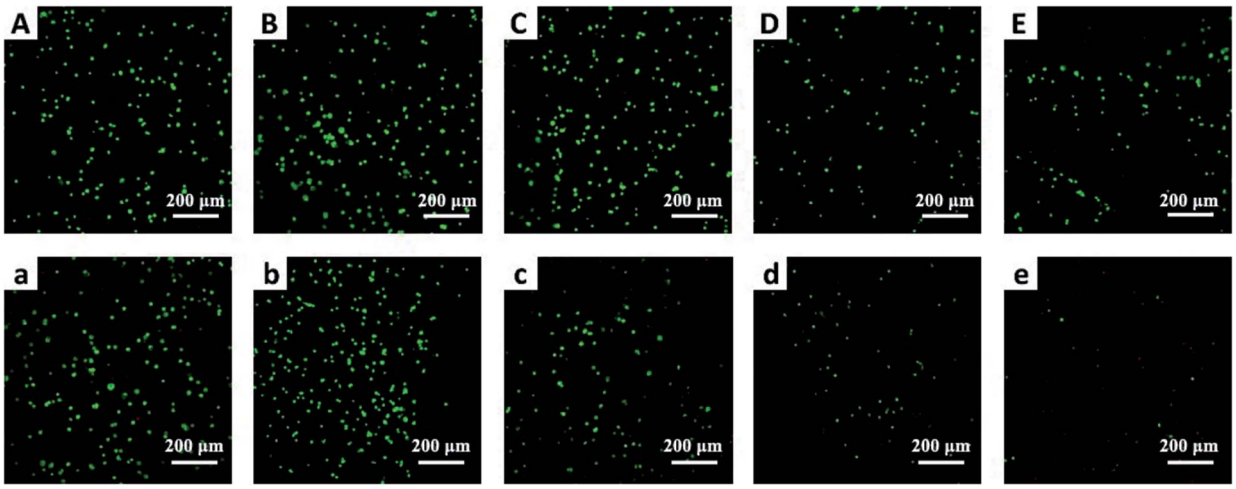

Fig. 8 Cell morphology observed using the laser scanning confocal microscope after culturing A-431 cells on the BCC and BCC_{60} composites for 24 h. (A and a) BC, (B and b) BCC_{60}-005, (C and c) BCC_{60}-010, (D and d) BCC_{60}-050, and (E and e) BCC_{60}-100.

the BCC_{60} composites possessed excellent anticancer abilities under light conditions, especially the BCC_{60}-100 composite. Compared to the other composites, with this composite, the death rate of the A-431 cells exceeded 80% and the best anticancer effects were achieved (control, BCC_{60}-005, BCC_{60}-010 and BCC_{60}-050). The anticancer ability increased gradually with increased concentrations of C_{60} (Fig. 7 b). In contrast to the light group, the anticancer ability of the dark group was relatively poor, which resulted from the anticancer different mechanism involved. For the cell apoptosis mechanism induced by C_{60}, previous studies have reported that there were two different mechanisms. In a dark environment, C_{60} nanoparticles can exhibit anticancer properties by piercing the cell membrane, causing the cytoplasm to leak, while in the light group, light irradiation compels C_{60} to react with oxygen from the atmosphere to generate abundant ROS, resulting in an improved anticancer efficacy.

To further verify the anticancer efficacy, living/dead staining was used to observe the morphology and cell death. As shown in Fig. 8, the results indicate that as the C_{60} concentration increased, the number of living cells (green) decreased and the number of dead cells (red) increased gradually, which is consistent with the CCK-8 results. However, the phototoxicity of BCC_{60} composites towards L929 cells (see Fig. S1 in the ESI†) as normal cells was much lower than that towards cancer cells, which demonstrated that the composites caused less damage to normal tissue. In summary, the BCC_{60} composites prepared using the dehydration-rehydration method displayed unique anticancer abilities, demonstrating their potential as a novel treatment for skin cancer in PDT.

Conclusion

In summary, novel BCC_{60} composites as multifunctional wound dressings were successfully fabricated using a novel dehydration-rehydration method and are expected to be used in PDT to treat skin cancer. A series of characterizations showed that C_{60} particles were uniformly distributed in the hyperfine three-dimensional network of BC, and the particle diameter was less than 100 nm, reaching a smaller size than previously reported in the literature, providing an improved method to solve the aggregation and poor solubility issues of C_{60} in polar solvents. More importantly, the BCC_{60} composites exhibited excellent antibacterial properties and a relatively high cell death rate toward the A-431 cell line when exposed to light, demonstrating their potential in multifunctional wound dressings for PDT applications.

Conflicts of interest

There are no conflicts to declare.

Acknowledgements

The authors gratefully acknowledge the financial support provided by the National Natural Science Foundation of China (51673071, 51232002 and 51603074), the Natural Science Foundation of Guangdong Province (2016A030313509), the Guangdong Scientific and Technological Project (2016B090918040, 2014B090907004) and the Guangzhou Important Scientific and Technological Special Project (201508020123).

Notes and references

1 W. M. Sharman, C. M. Allen and J. E. van Lier, *Drug Discovery Today*, 1999, **4**, 507–517.
2 P. Agostinis, K. Berg, K. A. Cengel, T. H. Foster, A. W. Girotti, S. O. Gollnick, S. M. Hahn, M. R. Hamblin, A. Juzeniene, D. Kessel, M. Korbelik, J. Moan, P. Mroz, D. Nowis, J. Piette, B. C. Wilson and J. Golab, *Ca-Cancer J. Clin.*, 2011, **61**, 250–281.
3 S. Yano, S. Hirohara, M. Obata, Y. Hagiya, S.-i. Ogura, A. Ikeda, H. Kataoka, M. Tanaka and T. Joh, *J. Photochem. Photobiol., C*, 2011, **12**, 46–67.
4 Z. Markovic, B. Todorovic-Markovic, D. Kleut, N. Nikolic, S. Vranjes-Djuric, M. Misirkic, L. Vucicevic, K. Janjetovic, A. Isakovic, L. Harhaji, B. Babic-Stojic, M. Dramicanin and V. Trajkovic, *Biomaterials*, 2007, **28**, 5437–5448.
5 P. Mroz, G. P. Tegos, H. Gali, T. Wharton, T. Sarna and M. R. Hamblin, *Photochem. Photobiol. Sci.*, 2007, **6**, 1139–1149.
6 H. Tsumoto, S. Kawahara, Y. Fujisawa, T. Suzuki, H. Nakagawa, K. Kohda and N. Miyata, *Bioorg. Med. Chem. Lett.*, 2010, **20**, 1948–1952.
7 Z. Markovic and V. Trajkovic, *Biomaterials*, 2008, **29**, 3561–3573.
8 T. Andersson, K. Nilsson, M. Sundahl and G. Westman, *J. Chem. Soc., Chem. Commun.*, 1992, **8**, 166.
9 K. Komatsu, K. Fujiwara, Y. Murata and T. Braun, *J. Chem. Soc., Perkin Trans. 1*, 1999, **1**, 2963–2966.
10 M. Akiyama, A. Ikeda, T. Shintani, Y. Doi, J. Kikuchi, T. Ogawa, K. Yogo, T. Takeya and N. Yamamoto, *Org. Biomol. Chem.*, 2008, **6**, 1015–1019.
11 L. F. Li, L. Ren, L. Wang, S. Liu, Y. R. Zhang, L. Q. Tang and Y. J. Wang, *RSC Adv.*, 2015, **5**, 25525–25531.
12 Q. Zhang, W. J. Yang, N. Man, F. Zheng, Y. Y. Shen, K. J. Sun, Y. Li and L. P. Wen, *Autophagy*, 2009, **5**, 1107–1117.
13 J. D. Fortner, D. Y. Lyon, C. M. Sayes, A. M. Boyd, J. C. Falkner, E. M. Hotze, L. B. Alemany, Y. J. Tao, W. Guo, K. D. Ausman, V. L. Colvin and J. B. Hughes, *Environ. Sci. Technol.*, 2005, **39**, 4307–4316.
14 S. Deguchi, R. G. Alargova and K. Tsujii, *Langmuir*, 2001, **17**, 6013–6017.
15 L. Bourre, S. Thibaut, A. Briffaud, N. Rousset, S. Eleouet, Y. Lajat and T. Patrice, *J. Photochem. Photobiol., B*, 2002, **67**, 23–31.
16 M. Gao, Q. Hu, G. Feng, N. Tomczak, R. Liu, B. Xing, B. Z. Tang and B. Liu, *Adv. Healthcare Mater.*, 2015, **4**, 659–663.
17 W. Hu, S. Chen, X. Li, S. Shi, W. Shen, X. Zhang and H. Wang, *Mater. Sci. Eng. C*, 2009, **29**, 1216–1219.
18 B. Ma, Y. Huang, C. Zhu, C. Chen, X. Chen, M. Fan and D. Sun, *Mater. Sci. Eng. C*, 2016, **62**, 656–661.
19 L. C. S. Maria, A. L. C. Santos, P. C. Oliveira, A. S. S. Valle, H. S. Barud, Y. Messaddeq and S. J. L. Ribeiro, *Polimeros*, 2010, **20**, 72–77.
20 B. Han and M. N. Karim, *Scanning*, 2008, **30**, 213–220.
21 D. Y. Lyon, L. K. Adams, J. C. Falkner and P. J. J. Alvarez, *Environ. Sci. Technol.*, 2006, **40**, 4360–4366.
22 H. S. Barud, S. J. L. Ribeiro, C. L. P. Carone, R. Ligabue, S. Einloft, P. V. S. Queiroz, A. P. B. Borges and V. D. Jahno, *Polim.: Cienc. Tecnol.*, 2013, **23**, 135–138.
23 C. Chen, D. Li, Q. Deng, Y. Wang and D. Lin, in *Advanced Materials and Information Technology Processing Ii*, ed. J. Q. Xiong, 2012, vol. 586, pp. 30–38.
24 Y. Lion, M. Delmelle and d. V. A. Van, *Nature*, 1976, **263**, 442.
25 J. Moan and E. Wold, *Nature*, 1979, **279**, 450–451.
26 J. S. Boateng, K. H. Matthews, H. N. E. Stevens and G. M. Eccleston, *J. Pharm. Sci.*, 2008, **97**, 2892–2923.
27 P. O. Ornellas, L. S. Antunes, K. B. Fernandes da Costa Fontes, H. C. Correa Povoa, E. C. Kuchler, N. L. Pontes Iorio and L. A. Alves Antunes, *J. Biomed. Opt.*, 2016, **21**(9), 090901.
28 J. Y. Nagata, N. Hioka, E. Kimura, V. R. Batistela, R. S. Suga Terada, A. X. Graciano, M. L. Baesso and M. F. Hayacibara, *Photodiagn. Photodyn. Ther.*, 2012, **9**, 122–131.